TECHNICAL MEMORANDUM

556

# Advances in Simulating Atmospheric Variability with the ECMWF model: From Synoptic to Decadal Time-scales

Peter Bechtold, Martin Köhler, Thomas Jung, Francisco Doblas-Reyes, Martin Leutbecher, Mark J. Rodwell, Frederic Vitart and Gianpaolo Balsamo

Research Department

Submitted to Quart. J. Roy. Meteor. Soc. The definitive version will be available on Wiley InterScience.

February 2008



European Centre for Medium-Range Weather Forecasts
Europäisches Zentrum für mittelfristige Wettervorhersage
Centre européen pour les prévisions météorologiques à moyen terme

Series: ECMWF Technical Memoranda

A full list of ECMWF Publications can be found on our web site under:
http://www.ecmwf.int/publications/

Contact: library@ecmwf.int



European Centre for Medium-Range Weather Forecasts
Shinfield Park, Reading, RG2 9AX, England

**Abstract**

Advances in simulating atmospheric variability with the ECMWF model are presented that stem from revisions of the convection and diffusion parametrizations. The revisions concern in particular the introduction of a variable convective adjustment time-scale, a convective entrainment rate proportional to the environmental relative humidity, as well as free tropospheric diffusion coefficients for heat and momentum based on Monin-Obukov functional dependencies.

The forecasting system is evaluated against analyses and observations using high-resolution medium-range deterministic and ensemble forecasts, monthly and seasonal integrations as well as decadal integrations with coupled atmosphere-ocean models. The results show a significantly higher and more realistic level of model activity in terms of the amplitude of tropical and extra-tropical mesoscale, synoptic and planetary perturbations. Importantly, with the higher variability and reduced bias not only the probabilistic scores are improved, but also the mid-latitude deterministic scores in the short-range and medium-range. Furthermore, for the first time the model is able to represent a realistic spectrum of equatorial Kelvin and Rossby waves, and maintains a realistic amplitude of the Madden-Julian oscillation (MJO) during monthly forecasts. The propagation speed of the MJO, however is slower than observed. The higher tropical tropospheric wave activity results also in better stratospheric temperatures and winds through the deposition of momentum.

The partitioning between convective and resolved precipitation is unaffected by the model changes with roughly 62% of the total global precipitation being of the convective type. Finally, the changes in convection and diffusion parametrizations resulted in a larger spread of the ensemble forecasts which allowed to decrease by 30% the amplitude of the initial perturbations in the ensemble prediction system.

# 1 Introduction

Forecasting the state of the atmosphere involves the prediction of a slowly evolving mean equilibrium state (also referred to as the climate) and the temporal and spatial variations about this state. Predicting the amplitude and phase of the planetary, synoptic and mesoscale perturbations in a deterministic and ensemble prediction system (EPS) is a challenging task.

The main physical processes that lead to the generation of kinetic energy in the atmosphere are the differential radiative heating and the convective heating (Haimberger and Hantel, 2000; Steinheimer et al., 2008). Latent heat release in deep convection excites among others equatorial Rossby, Kelvin and mixed Rossby-gravity waves. It has been demonstrated in numerous modelling studies (Slingo et al., 1994; Scinoccia and McFarlane, 2004; Lin et al., 2008) that the simulation of these waves in global models is very sensitive to the type of convective parametrization employed. Typically in these studies the simulated tropical variability increases with increasing resolved precipitation at the expense of the parametrized precipitation. An inadequate representation of the convective forcing and the associated equatorial waves has numerous consequences as errors project on the wavenumber 1 and 2 Madden-Julian oscillation (MJO) as well as on the stratospheric meteorology like the quasi-biennial oscillation (QBO) since these waves propagate upward and interact with the mean flow (Ricciardulli and Garcia, 2000; Horinouchi et al., 2003). These errors even affect mid-latitude meteorology through interaction with the midlatitude Rossby waves. In contrast to convection parametrization schemes, explicit models of deep convection tend to excite a larger and more realistic spectrum of waves. However these models are very expensive numerically, and either still have problems in representing a good mean atmospheric state (Khairoutdinov et al., 2005), or are mainly run on an aqua-planet (Nasumo et al., 2007) or on limited domains (Shutts, 2008), and therefore are not applicable yet to global numerical weather prediction.

The dissipation of kinetic energy mainly affects the high-wavenumber part of the motion spectrum. It is represented numerically in the horizontal and vertical diffusion schemes, and the parametrized convective momentum transport, but there is also implicit numerical diffusion inherent to the interpolations in the advection

scheme (Skamarock, 2004). The vertical diffusion scheme is of particular importance as it controls the surface friction/dissipation and acts on the tropospheric wind shear and temperature gradients which strongly influence the development of midlatitude synoptic systems (Badger and Hoskins, 2000; Håkånsson, 2002; Beare et al., 2003).

On 6 November 2007 ECMWF introduced a new model cycle, Cy32r3, into operations, which contained major modifi cations to the convection and vertical diffusion scheme. The impact of these changes on the simulated atmospheric mean state and atmospheric variations on a wide range of time scales, were relatively large compared to other model changes introduced in recent years. The aim of this article, therefore, is to give an overview of the performance of Cy32r3 compared to previous model cycles, in particular Cy32r2 that had received a substantial upgrade to the radiation scheme with a new shortwave code and the introduction of McICA (Monte Carlo Independent Column Approximation) (Morcrette et al., 2008). The model performance will be discussed especially in the light of the following well-known defi ciencies of previous versions of the ECMWF Integrated Forecasting System (IFS):

- A decrease in amplitude of tropical synoptic and planetary-scale activity within the fi rst ten days of the forecast.
- A slight underestimation of midlatitude synoptic activity in the medium range.
- A lack of growth of the ensemble spread in midlatitudes in the Ensemble Prediction System (EPS) that is compensated by choosing large initial perturbations.
- An underestimation in the total amount of precipitation and the amplitude of the annual cycle over the tropical continents.

The impact of the model changes is assessed using 44-years of $T_L159$ (125 km) uncoupled seasonal integrations and high-resolution $T_L799$ (25 km) 10-day deterministic forecasts with 91 vertical levels with a model top at 1 Pa, and by comparing the results to satellite and raingauge observations, operational analyses and reanalyses. In order to address the uncertainty with the reference data set, two reanalysis data sets are used when necessary, the ERA 40-year reanalysis (ERA40) (Uppala et al. 2005), and the new ERA Interim reanalysis that uses a 4D-Var assimilation scheme, an improved forecast model, and a variational bias correction scheme for satellite data. We also discuss the consequences of the model changes for the high-resolution $T_L399$/$T_L255$ (60 km/80 km) 15-day forcasts with the EPS and the $T_L159$ monthly forecasts, using constant and climatological sea surface temperatures, respectively. Finally, the effects on decadal simulations with a fully coupled atmosphere-ocean system are explored.

# 2 Features of model physics changes

## 2.1 Convection

Before the introduction of Cy32r3 the deep convection formulation in the IFS (see Bechtold et al. 2004 and references therein) was based on a mass flux approximation, which imposed a strong coupling between the convection and the large-scale dynamics through a mass entrainment proportional to the large-scale moisture convergence. This led to a diffi cult to control nonlinear feedback between the large-scale flow and the convection in terms of cloud top heights and rainfall amount. Furthermore, it has been recognised that the environmental humidity is a modulating factor in convective activity and MJO-like tropical variability (e.g. Grabowski and Moncrieff 2004), but that many convection parameterisations including the IFS scheme do not exhibit suffi cient

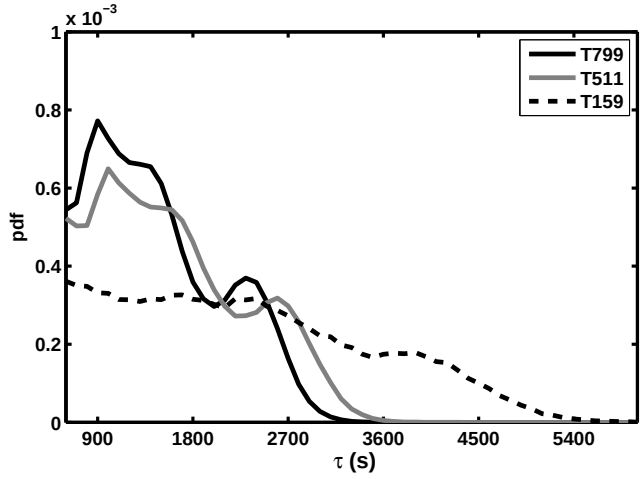


*Figure 1: Pdfs of CAPE adjustment time-scale for deep convection as sampled from forecasts with different resolutions.*

sensitivity with respect to environmental moisture (Derbyshire et al. 2004). Therefore, it was decided to make the scheme more sensitive to environmental moisture, and to remove any imposed large-scale control of the convection through the $\omega$ field (where $\omega = dp/dt$) or the moisture convergence, and to let the model find its own equilibrium[1].

The formulation for the variation with height of the convective mass flux $M$ includes contributions from turbulent and organised entrainment $\varepsilon$ and detrainment $\delta$

$$\frac{1}{M}\frac{\partial M}{\partial z} = \varepsilon - \delta = \varepsilon_{\text{turb}} + \varepsilon_{\text{conv}} - \delta_{\text{turb}} - \delta_{\text{conv}}. \tag{1}$$

In the new formulation the entrainment is specified as

$$\varepsilon = \underbrace{c_0}_{turb} F_\varepsilon + \underbrace{c_1 \frac{\bar{q}_l - \bar{q}}{\bar{q}}}_{org,deep,buoy>0} F_\varepsilon; \quad F_\varepsilon = \left(\frac{\bar{q}_l}{\bar{q}_{l,\text{b}}}\right)^2 \tag{2}$$

where $c_0$ and $c_1$ are tunable parameters of $O(10^{-4})$ with dimension $\text{m}^{-1}$, $\bar{q}$ is the environmental specific humidity, $\bar{q}_l$ and $\bar{q}_{l,\text{b}}$ are the saturation specific humidity at the parcel level and at cloud base, respectively, and $F_\varepsilon$ is a dimensionless vertical scaling function decreasing exponentially with height thereby mimicking an ensemble of clouds. The organised entrainment, active for deep convection if the parcel is buoyant, is therefore proportional to the relative humidity of the environment, providing a stronger sensitivity of the convection to environmental humidity (mid-level dry layers). The turbulent detrainment is simply a constant, whereas the organised detrainment is proportional to the reduction in updraught kinetic energy when the parcel buoyancy becomes negative.

Furthermore, the convective adjustment time is no longer a constant roughly equivalent to the resolution dependent model time step (720 s at $\text{T}_\text{L}799$, and 3600 s at $\text{T}_\text{L}159$), but it is set proportional to the convective turnover time scale

$$\tau = \frac{H}{\bar{w}_u^H} \quad \alpha; \quad \alpha = 1 + \frac{264}{n}, \tag{3}$$

[1]Formulating a suitable balance condition would be indeed very difficult (see also Žagar et al., 2005), and it can be shown through asymptotic expansion (Sobel et al., 2001) that the equations then either have wave like solutions or some radiative-convective equilibrium solutions that do not represent synoptic activity.

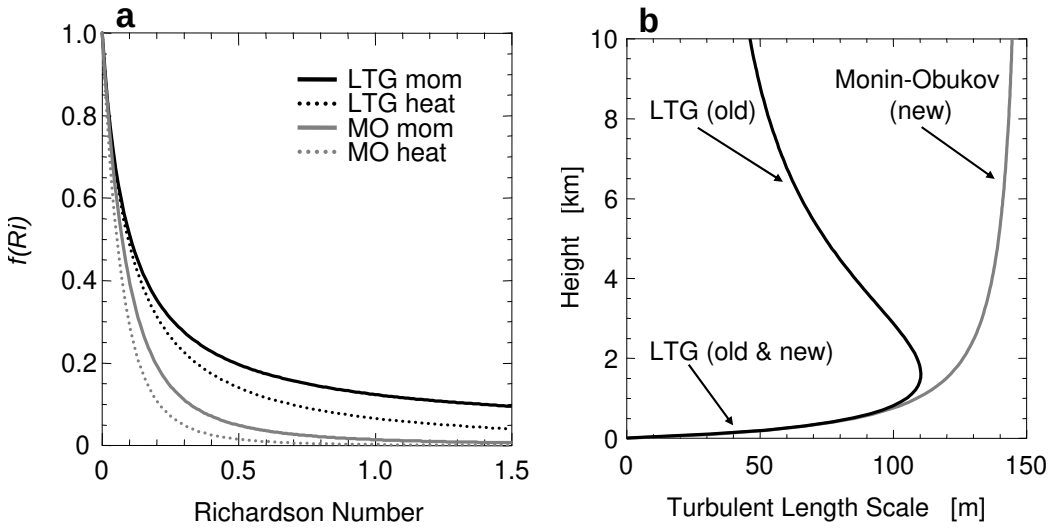


*Figure 2: LTG and Monin-Obukhov functional dependencies for heat and momentum (a), and corresponding turbulent length scales (b).*

where $\bar{w}_u^H$ is the updraught vertical velocity averaged over the cloud depth $H$, and $\alpha$ is a factor depending on the model truncation in spectral space $n$. Pdfs of the convective adjustment time-scale Equation (3) have been obtained from forecasts with different resolutions, and are depicted in Figure 1. The Pdfs appear to be of reasonable widths allowing for $\tau$ to vary between e.g. 600 and 3600 s at $T_L799$, in contrast to the single value of 720 s used before. We also experimented with a time-scale proportional to the time gravity waves propagate through the model grid, i.e. $\tau \approx c_\alpha \Delta x (gH)^{-1/2}$, with $g$ the gravity constant, $c_\alpha \approx 5$ a proportionality constant, and $\Delta x = \pi R n^{-1}$ the horizontal grid-spacing, with $R$ the earth radius. This formulation produced results that were rather similar but slightly degraded compared to that obtained with (3). For a discussion on the importance of the CAPE adjustment time-scale for simulating convective equilibria and the partitioning between resolved and convective precipitation the reader is referred to Done et al. (2006)

Finally, the vertical transport in the mass flux scheme has been formulated fully implicitly, hence is stable for large mass fluxes, and the convection scheme has been rendered quasi-linear. This does not only facilitate the optimisation of cloud parameters , e.g. $c_0$ and $c_1$, but the linearity property is an important prerequisite of the scheme for its use in the assimilation system where the tangent linear model must be a good approximation of the full nonlinear model (Lopez and Moreau, 2005).

## 2.2 Vertical diffusion

It has been realized for some time that for both stably stratified boundary layers and outside the boundary layer the model turbulent mixing, which is intended to reduce static and shear instabilities, is too strong. The consequence is that cloud-top inversions and therefore stratocumulus layers tend to be eroded, and the vertical shear of the wind is reduced. Following Beljaars and Viterbo (1999) the IFS uses a revised Louis et al. (1982) $K$-diffusion scheme (referred to LTG hereafter) for statically stable regimes corresponding to positive Richardson (Ri) numbers

$$K = \left| \frac{\partial U}{\partial z} \right| l^2 f_{\mathrm{LTG}}(Ri), \tag{4}$$

where $U$ represents wind speed, and $l$ the mixing length-scale.

The functionality $f_{\mathrm{LTG}}(Ri)$ has been artifi cially increased over laboratory-based Monin-Obukov values $f_{\mathrm{MO}}(Ri)$ to provide smoother vertical profi les and improve objective scores. This was justifi ed with a lack of knowledge of the stable boundary layer physics over complicated terrain. Yet, $f_{\mathrm{LTG}}(Ri)$ was applied throughout the troposphere. Figure 2(a) compares LTG and MO functionalities as a function of Richardson number. Note that for large static stability, as in inversions, LTG can still provide a non-negligible $K$, which in turn can erase the inversion. The old turbulent length scale (Figure 2(b)), goes linear with height near the surface up to a maximum value of 120 m, until it is reduced gradually to 30 m in the upper troposphere in order to avoid the erosion of the jet stream. We know that the large LTG diffusion coeffi cients above the boundary layer are unrealistic, and produce as undesired features too smooth profi les and the erosion of stratocumulus layers from the top. But it is also realised that the puzzle of why NWP needs larger than expected $K$'s in the stable boundary layer has not been solved. Therefore we adopted a two-layer approach. Close to the surface LTG functional dependencies are used and the turbulent length scale is linear with height $z$. In the free troposphere Monin-Obukov functional dependencies are used with a length scale of $\lambda_M$=150 m, and asymptotical behaviour in between (Figure 2(b))

$$\frac{1}{l\sqrt{f}} = \frac{1}{\kappa z\sqrt{f}} + \frac{1}{\lambda_M \sqrt{f_{\mathrm{MO}}}}, \tag{5}$$

where $\kappa$ is the von Karman constant. Note that no more length scale reduction in the upper troposphere is needed because of the smaller more realistic MO functional dependencies.

### 2.3 Other relevant system changes

Cy32r3 also contains two other major changes. A change in the soil hydrology scheme including a soil texture map and a new set of hydraulic properties for unsaturated soils, as well as a sub-grid surface runoff. These changes have a benefi cial impact on soil moisture and surface runoff. They also lead to a slightly moister analysis in the free atmosphere that more closely fi ts the observations. In addition Cy32r3 includes changes in the assimilation and observing system, and in particular a new bias correction scheme for radiosonde temperature and humidity data as a function of solar elevation and radiosonde type, and the use of additional sources of satellite data.

Changes to the forecasting system, particularly to the physical and numerical aspects, require thorough testing. It is impossible to cover all of them here, but some key diagnostics of the model climate and the quality and activity of the forecasts will now be discussed.

## 3 Model Climate

The sensitivity of the model climate to model formulation is studied using 13-month-long integrations with three different versions (Cy31r1, Cy32r2 and Cy32R3) of the atmospheric component of the ECMWF Integrated Forecasting System. A horizontal resolution of $\mathrm{T}_L159$ ($\approx 1.125^o$) was used with 91 levels in the vertical. Observed sea surface temperatures were prescribed as lower boundary conditions. Forecasts were started on 1 November of each of the years 1962–2005 (1990–2005) for Cy32r2 and Cy32r3 (Cy31r1).

Figure 3 compares the average observed precipitation from the Global Precipitation Climatology Project (GPCP), which is a combination of raingauge data and satellite-derived rainrates (Adler et al., 2003), for the December to March period with the values obtained from the seasonal integrations with Cy31r1, Cy32r2, and Cy32r3. Cy31r1 was operational between 12 September 2006 and 5 June 2007; it is also the cycle used in the Interim Reanalysis and the current seasonal forecasting system (known as System 3). Cy31R1 (and previous cycles)

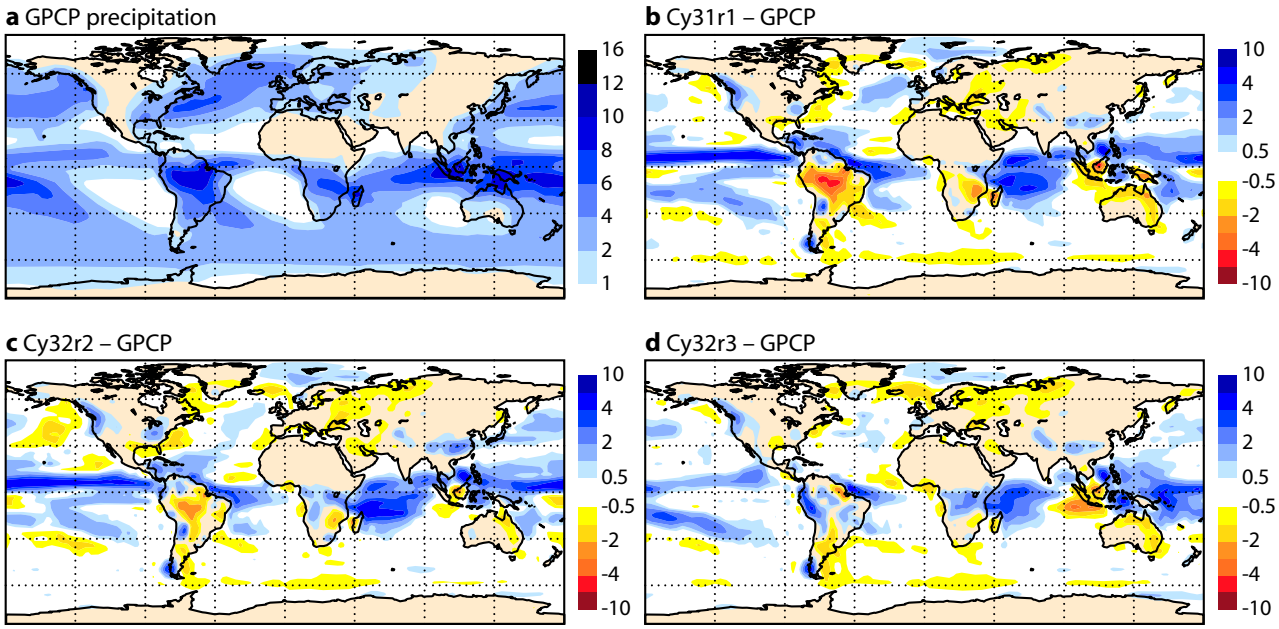


*Figure 3: (a) Average precipitation rate (mm/day) for winters (December–March) of the period 1990–2005 from GPCP. (b) Difference between the seasonal type integration at resolution $T_L159$ with Cy31r1 and GPCP. (c) and (d) As (b) but for Cy32r2 and Cy32r3.*

underestimates precipitation over the tropical continents, but overestimates precipitation over the Pacific Inter Tropical Convergence Zone (ITCZ) and the southern Indian Ocean. Cy32r2 with the revised radiation scheme reduces the precipitation biases, especially the convective rainfall over the tropical continents, due to stronger cloud-radiative feedback and a better description of surface shortwave heating. With Cy32r3 the overall rainfall distribution is further improved everywhere including a better representation of the land sea contrast. Convective precipitation in the West Pacific, however, is overestimated by all three model versions. The global average precipitation rate is reduced from 3.0 mm/day to 2.9 mm/day which is more in line with observational estimates. Furthermore the tropical troposphere in Cy32R3 is significantly moister between about 850 and 600 hPa (not shown). However, the partitioning between convective and stratiform (resolved) precipitation is essentially the same for the different model versions, with the convective contribution to the total tropical (global) precipitation amounting to 75% (62%). The rainfall changes in Cy32r3 not only reflect a local effect due to the changes in convection, but also reflect changes in the large-scale circulation and the transport of moisture from the subtropics to tropical regions. Finally, we take a closer look at the precipitation rates averaged over the Amazon basin and parts of the Andes (Figure 4). It is noticeable that compared to a special set of raingauge data (Betts et al., 2005) Cy32r3 also improves the amplitude of the annual cycle of rainfall which has been rather flat in previous IFS cycles.

The tropical wave activity in the long integrations is effectively evaluated using wavenumber-frequency for either Outgoing Longwave Radiation (OLR), 850 hPa winds or 200 hPa velocity potential (e.g. Wheeler and Kiladis 1999). Theory (Gill, 1980) shows that an equatorial local heat source generates, amongst others, westward moving Rossby waves with phase speeds around 5 m $s^{-1}$, and eastward moving Kelvin waves with phase speeds of 15–20 m $s^{-1}$. Figure 5 compares the wavenumber-frequency spectra of the predicted OLR averaged over the latitude band 10°S-10°N to spectra of the OLR observed by NOAA satellites. Notice the relative lack of power in the easterly modes (Kelvin waves) in Cy31r1 and Cy32r2. However, Cy32r3 realistically represents both Rossby and Kelvin mode activity, but now somewhat overestimates the power at low frequencies and wavenumbers. The dominant mode in the OLR spectrum within the positive wavenumber 1–2 band and

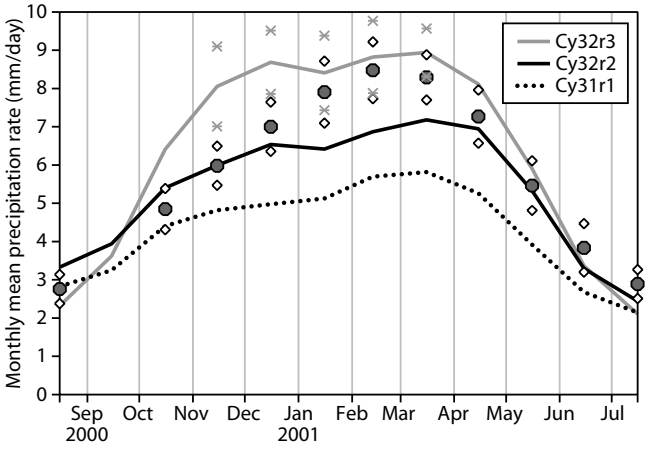


*Figure 4: Annual cycle of monthly mean precipitation rates (mm/day) for Amazonia obtained from a one-year integration of a four-member $T_L159$ ensemble with Cy31r1, Cy32r2 and Cy32r3. The raingauge observations are denoted by circles and the standard deviations of monthly mean precipitation rates for the observations and Cy32r3 are denoted by diamonds and crosses, respectively.*

frequency range of 20–60 days (0.05–0.016 cycles per day in Figure 5) is a signature of the MJO (see also the discussion in Section 6). The increased tropical wave activity in Cy32r3 also has a beneficial impact on temperatures and winds in the tropical stratosphere and mesosphere as Rossby and Kelvin waves propagate vertically through the atmosphere. However, the increased wave activity (and associated momentum transfer during wave breaking events) is not sufficient to produce the observed Quasi-Biannual Oscillations (QBO) in the modelled stratospheric zonal winds in the tropics (not shown).

After having established the largely positive impact of the revised convection and diffusion parameterization in the tropics in the following the impact on the model climate in the Northern Hemisphere extratopics will be discussed. Average zonal mean zonal winds are shown in Figure 6 for winters (December–March) of the period 1988–2001 and ERA40, ERA Interim, Cy32r2 as well as Cy32r3. Evidently, Cy32r2 (and also Cy31r1, not shown) produces a too strong polar vortex compared to the two reanalysis products. Cy32r3, on the other hand, simulates much more realistic stratospheric zonal mean zonal winds. Also shown in Figure 6 are Eliassen-Palm (EP) flux vectors and their divergence for stationary planetary waves. For Rossby waves, Eliassen-Palm vectors indicate the net wave propagation; negative (positive) values of EP flux divergence in the stratosphere indicate a reduction (acceleration) of zonal mean zonal winds by breaking stationary planetary waves (e.g. Edmon et al. 1981). The two reanalysis products show that tropospheric stationary planetary waves propagate upward into the stratosphere where they break and slow down the strength of the stratospheric polar vortex. In fact, the overestimation of the strength of the stratospheric polar votex in Cy32r2 might at least partly be explained by a lack of stationary planetary wave breaking in the middle and lower stratosphere. Zonal mean zonal winds and EP flux diagnostics for Cy32r3 show better agreement to the two reanalysis products throughout the stratosphere. Furthermore, Figure 6 reveals an improvement in the stationary planetary wave structure throughout the troposphere for Cy32r3 compared to Cy32r2.

The observed number of long-lived and mobile extratropical cyclones during boreal winter is shown in Figure 7a. Here the method used for identification and tracking of extratropical cyclones is exactly the same as described in Jung et al. (2006). The two main storm tracks in the North Atlantic and North Pacific region are clearly captured by the cyclone number diagnostic (Figure 7a). Furthermore, an increased number of cyclones are found inthe wake of major Northern Hemisphere mountain ranges such as the Rocky Mountains and the Alps. Systematic error of the number of cyclones in Cy32r2 (Figure 7b) is broadly consistent with those reported for an earlier model cycle (Cy29r1, Jung et al., 2006), that is, (i) a too northerly position of the North

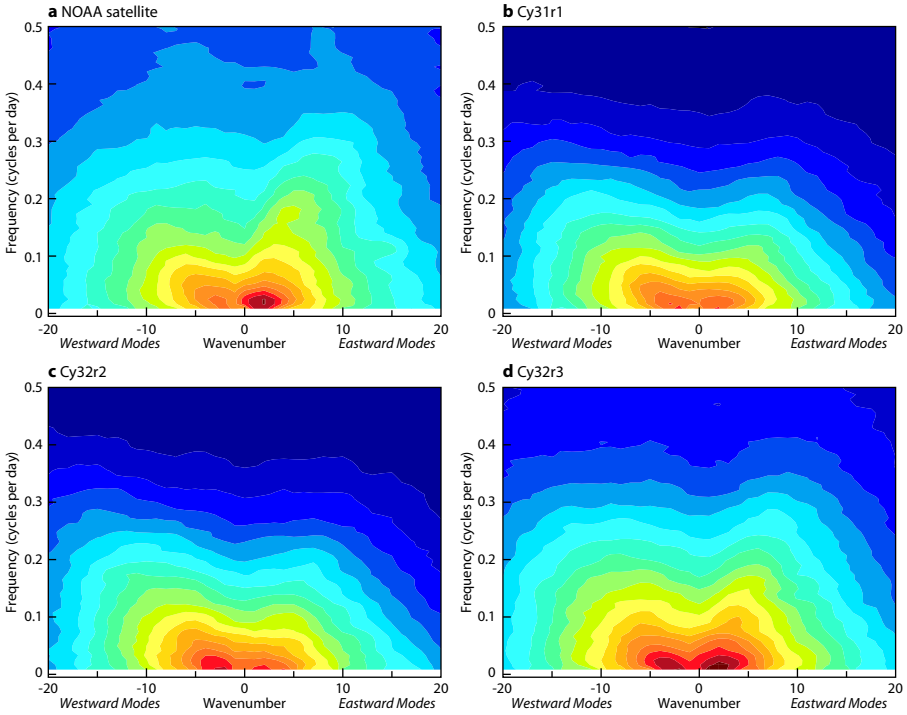


*Figure 5: Power in the frequency (cycles per day) and wavenumber space for the Outgoing Longwave Radiation (OLR) in the 10°S-10°N tropical region from (a) NOAA satellite observations. Also shown are corresponding results for 15 winter (December–March, 1990–2005) runs with (b) Cy31r1, (c) Cy32r2 and (d) Cy32r3. Contour intervals increase quadratically from 0.4 to 400.*

Pacifi c storm track, (ii) underestimation of the number of cyclones in the Kuroshio and Gulf Stream region, (iii) underestimation of cyclones around Greenland, (iv) underestimation of cyclones in the easter Mediterranean Sea and (v) overestimation of the number of cyclones in the eastern North Atlantic, which is consistent with the underestimation of Euro-Atlantic blocking events (e.g. Jung, 2005). Most of the above-mentioned model problems have disappeared in Cy32r3 (Figure 7c). Improvements in the Euro-Atlantic region can largely be explained by a better representation of Euro-Atlantic blocking events, which may partly be related to a more realistic strength of the stratospheric polar vortex (Boville 1984; Jung and Barkmeijer, 2006). Improvements in the North Pacifi c storm track are consistent with a more realistic stationary waves structure in Cy32r3 (not shown).

# 4 Deterministic forecasts

## 4.1 Model activity and deterministic scores

Cy32r3 has been tested in the full $T_L799$ (25 km) resolution analysis/forecast cycle for ten months from January to October 2007. The relative activity of a model can be defi ned as the standard deviation of forecast anomalies divided by the standard deviation of observed (i.e. analysed) anomalies from the ERA40 climatology. Figure 8 shows the relative activity as a function of forecast lead time for forecasts with model cycle Cy32r2 that was operational between 5 June 2007 and 5 November 2007, and cycle Cy32r3 that became operational on 6 November 2007 and which is the topic of this article. Relative activity is shown for 850 hPa temperatures in the northern and Southern Hemispheres (poleward of 20°), and for 925 hPa temperatures in the tropics. The

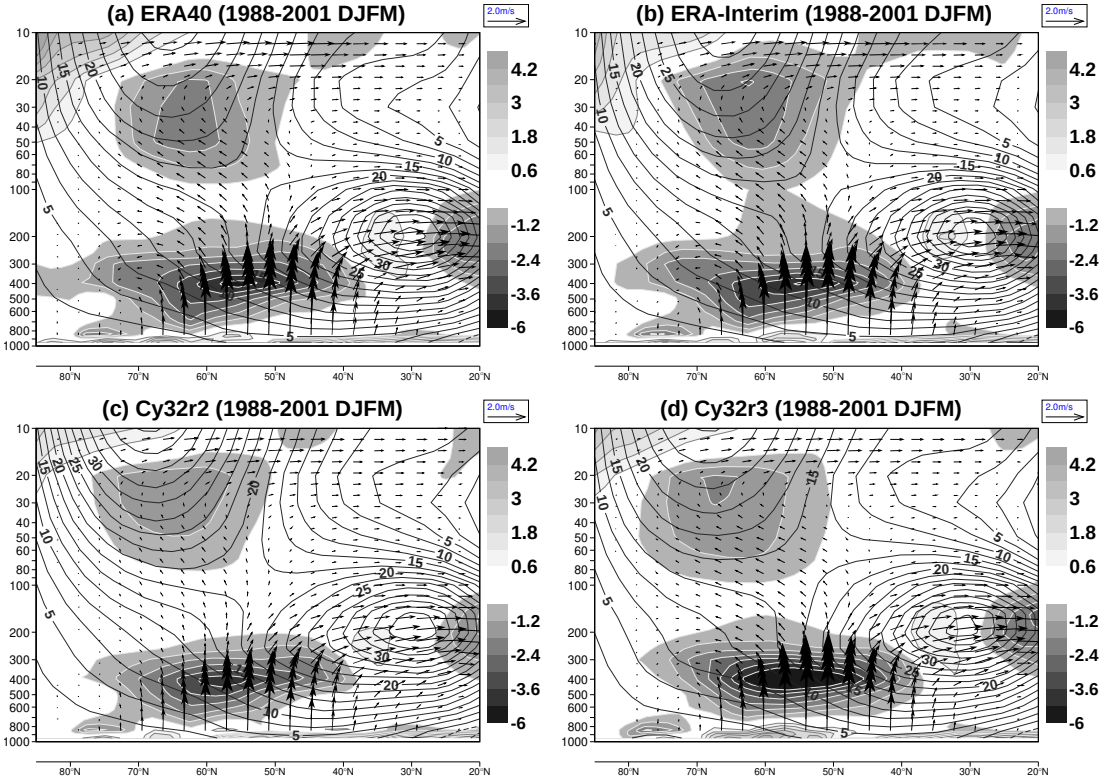


*Figure 6: Zonal mean zonal wind (contour interval is 2.5 m $s^{-1}$) and Eliassen-Palm flux vectors and divergence (shaded in m $s^{-1}$ $day^{-1}$) associated with stationary planetary waves for winters (December–March) of the period 1988–2001: (a) ERA40, (b) ERA Interim, (c) Cy32r2 and (d) Cy32r3. The Eliassen-Palm flux vectors are defined as in Peixoto and Oort (1992, p.388) as* $[-R\cos\phi \quad \overline{u^*v^*}, fR\cos\phi \quad \overline{v^*\theta^*}(\partial\theta/\partial p)^{-1}]$*, where* $f$ *is the Coriolis parameter,* $\phi$ *is latitude,* $\theta$ *the potential temperature, and stars denote anomalies from the zonal mean.*

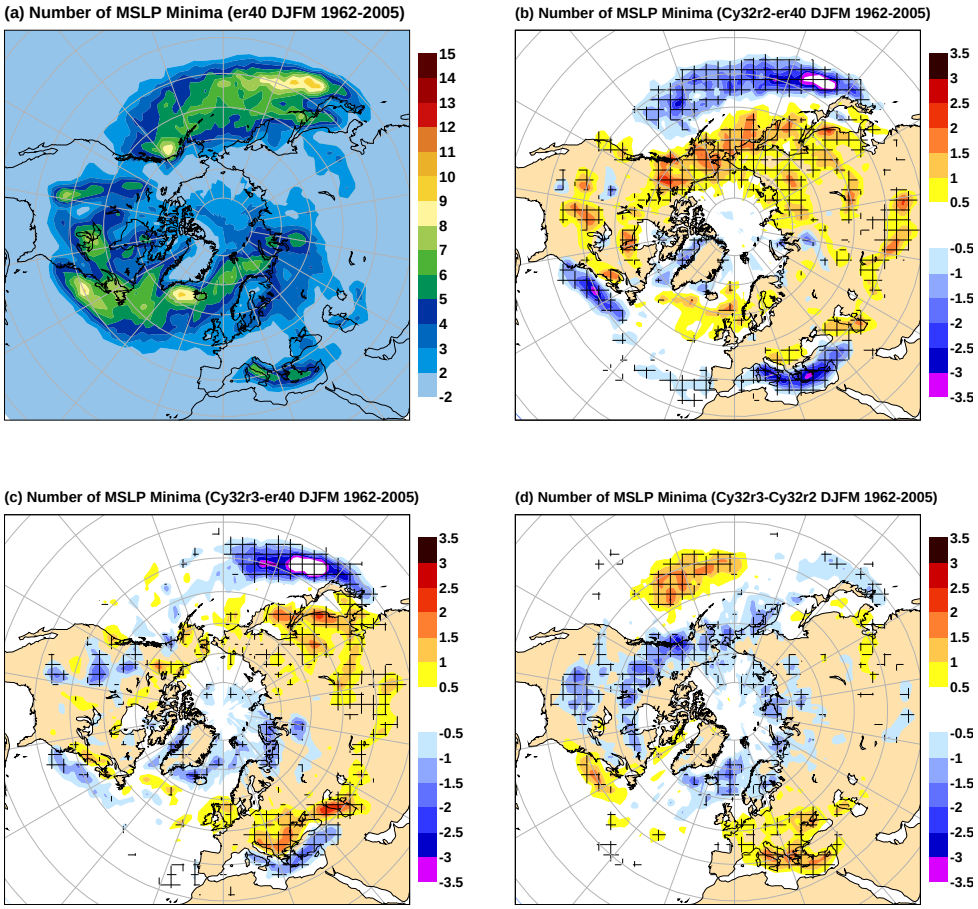


*Figure 7: (a) Number of cyclones per winter season from the ERA40 with lifetimes of two days and longer which migrated a minimum distance of 1000 km. Difference between (b) Cy32r2 and ERA40, (c) Cy32r3 and ERA40, and (d) Cy32r3 and Cy32r2. Results are based on winters (December–March) of the period 1962–2005, with the hatched areas standing for statistically significant differences.*

850 hPa temperature variations in midlatitudes are a good measure of cold and warm advection associated with synoptic systems, whereas tropical temperatures variations at the 925 hPa level are representative of the low-level convergent/divergent circulations. Figure 8 indicates that Cy32r2 slightly underestimates midlatitude atmospheric activity, but more importantly underestimates activity in the tropics. This problem was also present in all previous cycles. In contrast, in Cy32r3 model activity is close to the climatology within the first ten days in both the midlatitude and tropical regions. Indeed the dots show that the activity is significantly better compared to Cy32r2 at the 95% confidence level, based on a two-sided Student T-test.

Figure 9 shows mean forecast performance based on spatial correlations between forecast anomalies and analysis anomalies from all available 00 and 12 UTC forecasts. Results are shown for 1000 and 500 hPa heights and for the northern and Southern Hemispheres. In the Southern Hemisphere Cy32r3 improves over Cy32r2 at all lead times. As indicated by the dots in Figure 9 these improvements are statistically significant. In the Northern Hemisphere the improvements are smaller and only statistically significant during the first five days. Beyond day 5, Figure 8 gives an indication of a slight over-activity in Cy32r3 in the Northern Hemisphere and this seems to compromise somewhat the Northern Hemishere scores in the medium range. To put these results into perspective we refer to Simmons and Hollingsworth (2002) who reported that during the last decade the improvement in predictability in sea-level pressure and 500 hPa geopotential height amounts to about 1-day in the Northern Hemisphere and about 2-days in the Southern Hemisphere.

### 4.2 Satellite imagerie and mesoscale variability

Since August 2005 the IFS has produced forecast-generated satellite images. These correspond to brightness temperatures (BTs) computed from the RTTOV (Radiative Transfer model for TOVS, ATOVS and Other Vertical sounders) in the 10.8 $\mu$m infrared band and the 6.2 $\mu$m water vapour band that can be directly compared to observed BTs from Meteosat 8 and Meteosat 9. As the infrared BTs have values that are very close to the actual cloud top temperatures, the synthetic images are an excellent tool for indirectly verifying the model clouds (cloud cover and condensate content) and the synoptic and convective activity associated with cloud systems. Figure 10(a) shows the infrared satellite image from Meteosat 9 for 1 July 2007 for large parts of Europe and North Africa, with the corresponding six-hour forecast images with Cy32r2 and Cy32r3 given in Figures 10(b) and 10(c). Generally the model gives a good representation of the midlatitude synoptic cloud systems, but has more difficulty with tropical convection. It seems, however, that Cy32r3 reproduces more realistic tropical convection associated with the African Easterly Waves between the equator and 5°N (two waves are apparent in Figure 10). As a quantitative verification, time series from 15 June to 14 July 2007 of spatial correlations and mean errors between daily 6-24 hours forecast and observed infrared BTs are plotted in Figure 11. The errors exhibit a diurnal cycle with the largest positive biases and lowest correlations occurring during night. This indicates that the forecasts have difficulty in producing long-lived convective systems that extend into the night. With Cy32r2 the average spatial correlation between observed and forecast BTs is about 0.5. Cy32r3 slightly improves this correlation, and in particular improves the warm bias in the forecast which becomes smaller than 1 K. The improvement in Cy32r3 can be linked to the more intense continental convection and larger upper-level convective detrainment, producing more and colder anvil clouds, and to an improved analysis using the new radiosonde bias correction scheme. Applying the same type of verification for Europe (not shown), the two cycles produce nearly identical results, but correlations between observed and forecast BTs are much higher with values around 0.8.

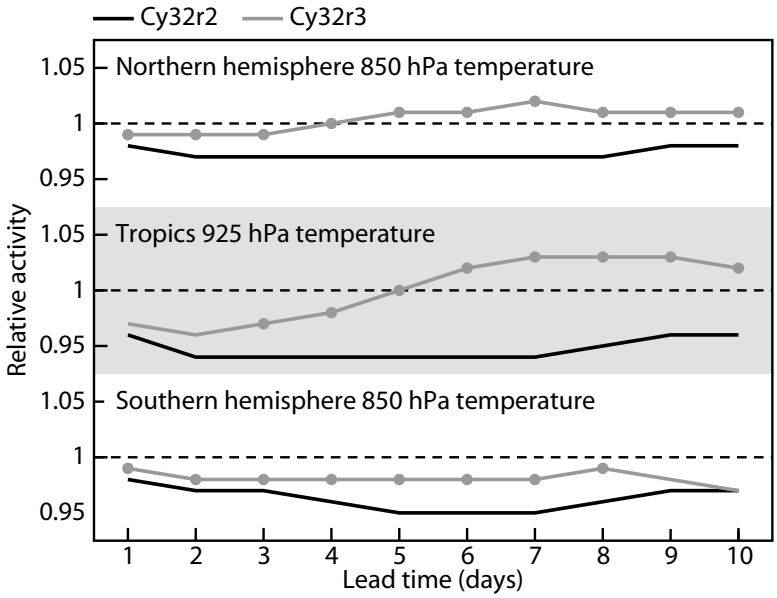


*Figure 8: Relative activity in Cy32r2 and Cy32r3 as a function of forecast lead time for 850 hPa temperatures in the northern and Southern Hemispheres, and tropical temperatures at 925 hPa. The relative activity is defined as the ratio between the standard deviation of forecast anomalies and the standard deviation of anomalies from an ERA40 based climatology. The grey dots denote improvements that are significant at the 95% confidence level.*

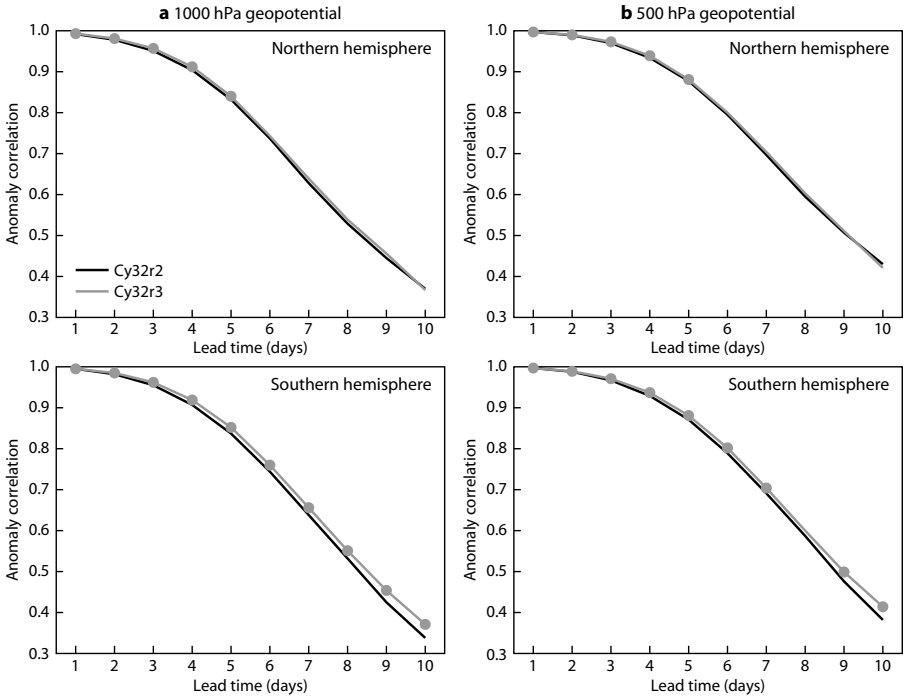


*Figure 9: Mean spatial anomaly correlations for Cy32r2 and Cy32r3 as a function of forecast lead time for the Northern Hemisphere (20°N-90°N, top) and Southern Hemisphere (20°S-90°S, bottom) and for 1000 hPa geopotential heights (left) and 500 hPa geopotential heights (right) for January to October 2007. The dots denote improvements that are significant at the 95% confidence level using a 2-sided Student's T-test taking autocorrelation into account. Over 400 forecasts are used in the analysis. Anomalies are relative to ERA40. Scores are calculated on a T63 (300 km) Guassian grid.*

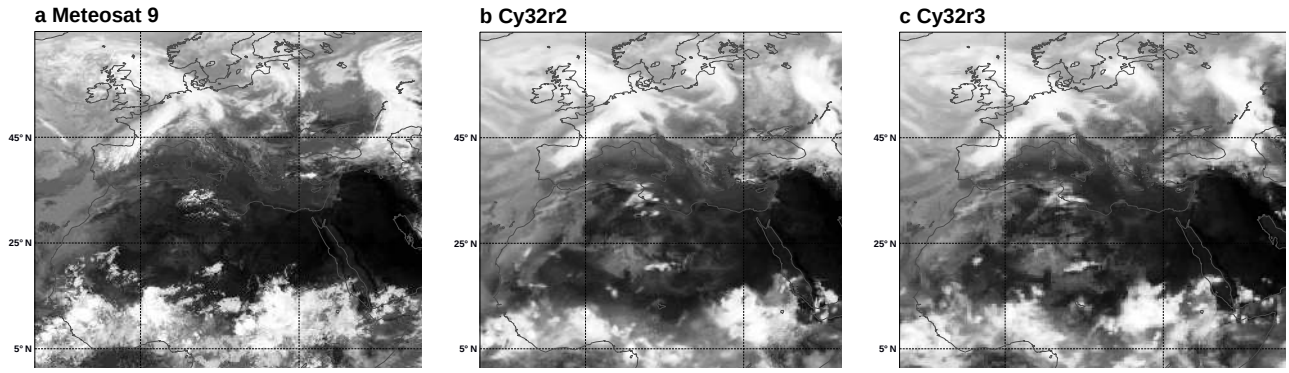


*Figure 10: (a) Observed infrared 10.8 μm brightness temperatures (BTs) from Meteosat 9 for 06 UTC on 1 July 2007. (b), (c) The corresponding RTTOV generated BTs from six-hour forecasts with Cy32r2 and Cy32r3.*

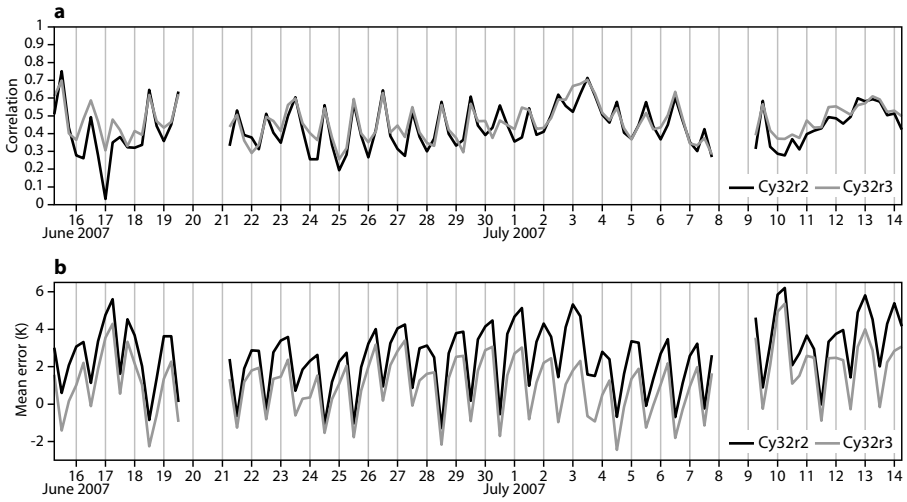


*Figure 11: Time series from 15 June to 14 July 2007 of (a) correlation and (b) mean error of forecast synthetic 10.8 μm BTs obtained with Cy32r2 and Cy32r3 against Meteosat 9 observations. Data points correspond to daily forecasts with lead times 6, 12, 18 and 24 hours that are area-averaged over Central Africa (20°S-20°N, 20°W-30°E); missing data are blanked.*

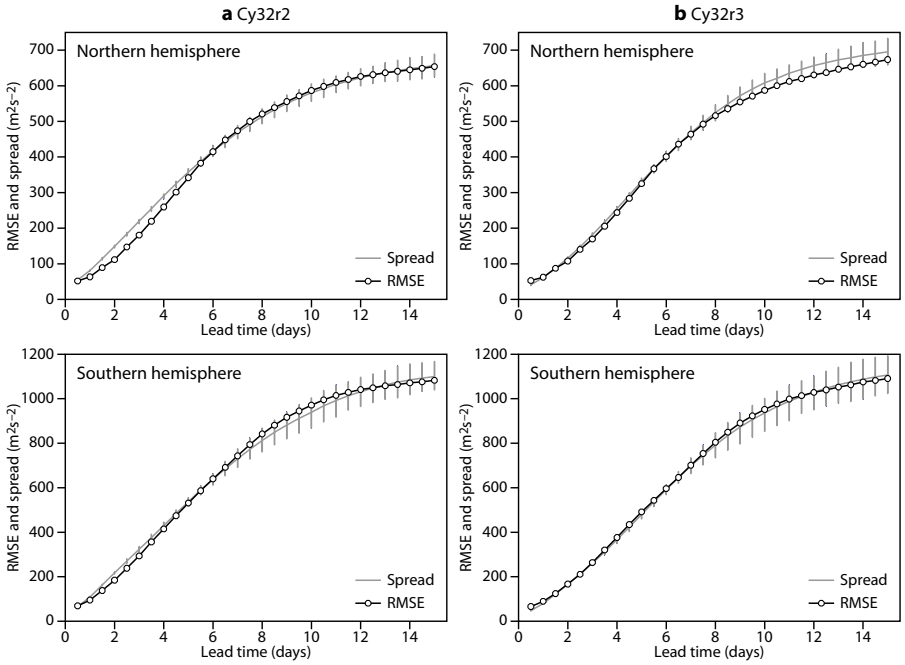


*Figure 12: Ensemble standard deviation (spread) and ensemble mean RMS error (RMSE) as a function of forecast lead time for 500 hPa geopotential for the Northern Hemisphere (20°N-90°N, top panel) and Southern Hemisphere (20°S-90°S, bottom panel) for (a) Cy32r2 and (b) Cy32r3. Statistics are based on 69 cases during June to September 2007. The vertical bars are confidence intervals based on bootstrapping the dates in the sample of cases. If the RMSE falls within the bars, the ensemble is not significantly over- or under-dispersive (the probability of the RMSE being above or below the bar by chance is 1%).*

# 5 The Ensemble Prediction System

The characteristics of perturbation growth in the EPS (Leutbecher and Palmer 2008; Buizza et al. 2005) were signifi cantly changed due to the convection and vertical diffusion changes in Cy32r3. In a statistically consistent ensemble, the RMS error of the ensemble mean (computed over a suffi ciently large sample) should match the ensemble standard deviation. For Cy32r2, the ensemble spread and the ensemble mean RMS error agree well from about day 5 onwards (Figure 12(a)). However, the good agreement from day 5 can only be achieved by using a large initial perturbation amplitude which results in an over-dispersive ensemble during the earlier forecast ranges. Initial experimentation with the new convection and diffusion scheme indicated that the physics changes produce a signifi cant increase in the ensemble standard deviation. This offered the opportunity to reduce the initial perturbation amplitude in order to improve the agreement between spread and ensemble mean RMS error at all forecast ranges. First, a reduction of the initial perturbation amplitude by 20% was tested in a sample of 13 summer and 13 winter cases. Results indicated that a further reduction of the initial perturbation amplitude was required and it was decided to reduce the initial perturbation amplitude by 30% in Cy32r3. The faster perturbation growth due to the convection and diffusion changes, together with the reduced initial perturbation amplitude, results in an improved overall agreement between ensemble spread and ensemble mean RMS error in Cy32r3 (Figure 12(b)). The EPS no longer suffers from an over-dispersion in the early forecast ranges. The EPS evaluation for Cy32r3 is based on nearly ten weeks of daily ensemble forecasts from June, August and September 2007. The improved match between ensemble spread and ensemble mean RMS error are statistically signifi cant (see confi dence intervals in Figure12). The Ranked Probability Skill Score (RPSS) (see Wilks 1995, pp. 269 ff.) evaluates the mean squared error of the predicted cumulative distributions. In terms of this score the probabilistic prediction of 850 hPa temperature is signifi cantly better in Cy32r3 than

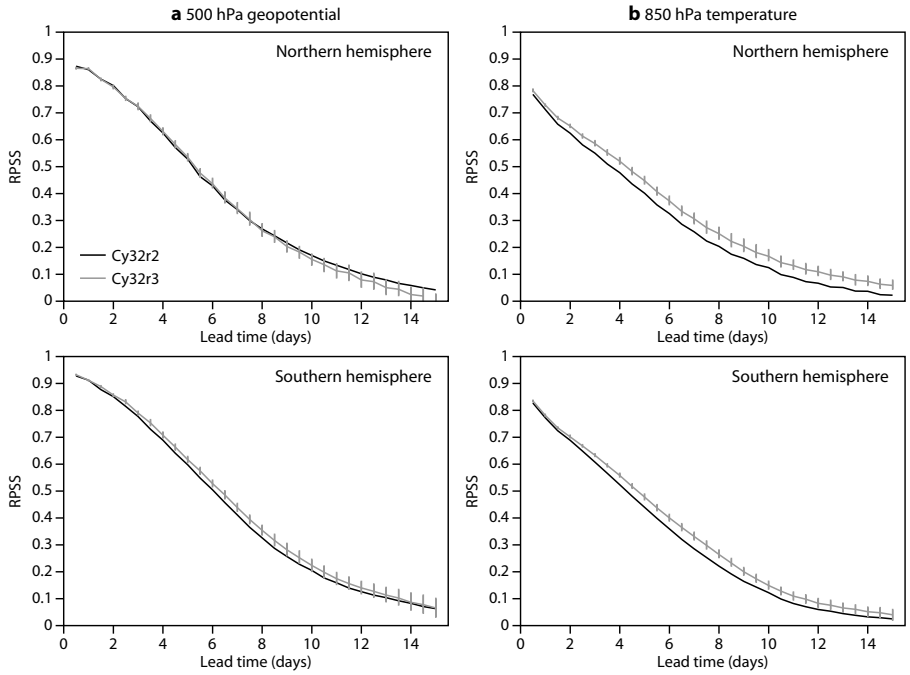


*Figure 13: Ranked Probability Skill Score (RPSS) for Cy32r2 and Cy32r3 as a function of forecast lead time for the Northern Hemisphere (20°N-90°N, top panel) and Southern Hemisphere (20°S-90°S, bottom panel) for (a) 500 hPa geopotential and (b) 850 hPa temperature. The RPSS is determined for ten climatologically equally likely categories. Cy32r3 is significantly better (worse) than Cy32r2 at the 99% level if the black curve lies below (above) the vertical bars.*

its predecessor in both hemispheres and at all forecast ranges (Figure 13(b)). For 500 hPa geopotential, the impact of Cy32r3 is neutral in the Northern Hemisphere and positive in the Southern Hemisphere (Figure 13(a)). Note, that there is no simple relationship between the probabilistic skill and the deterministic skill of the ensemble mean. For instance, while the impact of Cy32r3 on the RPSS of 500 hPa geopotential in the Northern Hemisphere is neutral, Cy32r3 has a positive impact on the RMS error of the ensemble mean (again with more than 99% statistical significance). By the same token, the impact on the RMS error of the ensemble mean is neutral for 850 hPa temperature in the Northern Hemisphere while a statistically significant positive impact was noted for the RPSS.

# 6 Monthly forecasts and the Madden-Julian Oscillation

The MJO is the dominant mode of intraseasonal variability in the tropical atmosphere. Statistical models suggest that it is an important source of predictability (Wheeler and Weickmann 2001). Therefore, it is important that the monthly forecasting system accurately predicts its onset and evolution. To assess the skill of the monthly forecasting system to predict an MJO event, 32-day coupled ocean-atmosphere integrations using a five-member ensemble have been performed for each day between 15 December 1992 and 31 January 1993 (46 ensemble integrations); this period corresponds to the Intense Observing Period (IOP) of TOGA-COARE. The MJO is diagnosed in these integrations using a method based on the technique of Wheeler and Hendon (2004). Combined Empirical Orthogonal Functions (EOFs) of OLR, 200 hPa velocity potential and 850 zonal wind averaged over 10°N-10°S are calculated using ECMWF operational data between 2002 and 2004. The EOF analysis is performed on the anomalies relative to the seasonally evolving climatology. The first two EOFs, which represent 18% and 17% of the variance respectively, describe variations associated with the MJO.

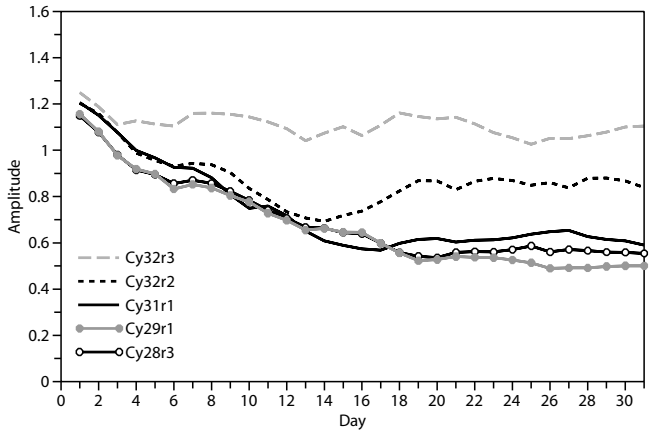


*Figure 14: Amplitude of the first combined EOF of Outgoing Longwave Radiation (OLR), 200 hPa velocity potential and 850 hPa zonal wind as a function of forecast lead time from Cy28r3 to Cy32r3. The amplitude constitutes an average over each ensemble member and the 46 cases, with its initial values corresponding to the ERA40.*

Observations and forecasts are then projected onto these two EOFs. Different cycles from Cy28r3 onward (operational implementation 29 April 2004) have been run for the control period in order to assess the impact of changes in the physics on the skill of the monthly forecast system to predict an MJO event. Figure 14 shows the amplitude of Principal Component 1 (PC1) averaged over the 46 integrations and the five members of the ensemble as a function of the forecast time. Results are similar for Principal Component 2 (PC2). Before Cy32r3, all versions of the IFS shared the same problem, namely a rapid drop in the amplitude of PC1 and PC2 as can be seen in Figure 14. For instance, with Cy28r3 the MJO loses 25% of its amplitude after only five days of integrations, about 33% by day 10, and about 50% by day 20. This means that the impact of the MJO on the extra-tropics was likely to be strongly underestimated in those cycles. On the other hand Figure 14 shows that Cy32r3 is the first IFS cycle able to sustain the amplitude over the whole period of the integration. This is an important result since it implies that, for the first time, the monthly forecasting system may now be able to adequately represent the impact of the MJO on the extra-tropics. Figure 15 illustrates the progress made in the representation of the MJO with the IFS. In Cy28r3 the OLR anomalies are very weak by day 15. Each new cycle increases the amplitude of the OLR anomalies (results are similar for velocity potential at 200 hPa and zonal wind at 850 hPa), and with Cy32r3 the OLR anomalies by day 15 are as intense as in ERA40. However, the propagation of the MJO with Cy32r3 is slower than in the analysis. In particular, the model has some difficulty propagating the convection from the Indian Ocean to the Pacific, and instead tends to maintain the convection over the Indian Ocean for too long. The reason for this deficiency is yet unclear, but it may be related to an overestimation of convective precipitation over the maritime continent and/or as advocated by Masunaga (2007) to wave interference between the incoming eastward propagating Kelvin wave and outgoing westward propagating Rossby waves.

# 7 Decadal simulations

ECMWF also assesses the atmosphere-ocean coupled seasonal forecast system using decadal integrations. Several IFS cycles have been used to assess the benefit of improvements in the atmospheric component. Sets of three-member ensemble 10-year simulations have been carried out using the IFS/HOPE coupled model (Anderson et al., 2007). The simulations start on the first of November 1994 from ERA40 atmospheric and soil conditions and from the ORA-S3 ocean data (Balmaseda et al., 2008). The ensemble is generated as described in Berner et al. (2008), with perturbations in the ocean initial conditions and atmospheric singular vectors.

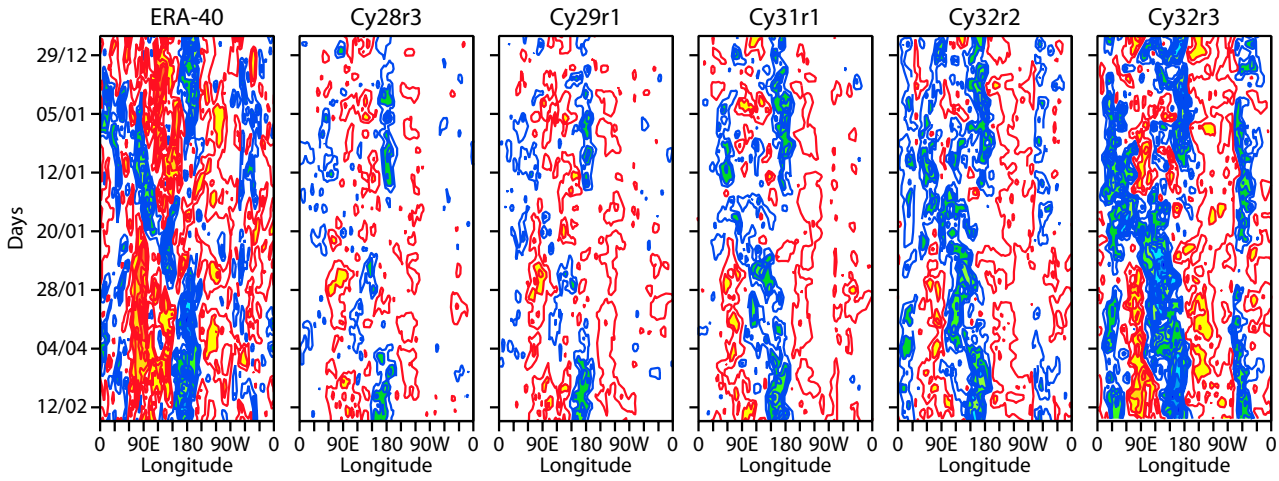


*Figure 15: Hovmöller diagrams of the averaged Outgoing Longwave Radiation (OLR) between 10°S and 10°N from 29 December 1992 to 15 February 1993 as analysed by ERA-40 and obtained from forecasts with Cy28r3 to Cy32r3 using concatenated daily forecasts with a 15 day lead time. Red shading denotes warm OLR anomalies (negative phase of the MJO) and blue shading cold anomalies (convectively active phase of the MJO).*

Sea-ice is kept at climatological values. Annual concentrations of well-mixed greenhouse gases are specified, but no anthropogenic or volcanic aerosols are included during the integration.

For seasonal and climate prediction, ideally model drift should be kept to a minimum. While some systems use corrections in the fluxes exchanged between the atmosphere and the ocean, a more desirable approach consists in improving the physical processes in the model that might lead to a more realistic basic state. A step forward to attain this goal has been achieved with Cy32r3. Figure 16 shows time series of the anomalies of sea surface temperature over the tropical Pacific (125°E–80°E,30°N–30°S) for ERA40 and the simulations. The tropical Pacific is a key region in seasonal and interannual forecasting due to its link to the El Niño-Southern Oscillation (ENSO) phenomenon. The anomalies have been computed as the difference between monthly values and the mean seasonal cycle from ERA40 over the period 1970–2000. Figure 16 illustrates the drift in the simulations, which is too strong after the first year for Cy31r1, reaching values close to 2 K. The drift is reduced in Cy32r2, although there is a fast decrease in temperature after the first year. The Cy32r2 values amount to around 1 K after two years of simulation, whereas Cy32r3 further reduces the differences with the ERA40 climatology to a value below 1 K. Cy32r3 is also the first cycle that shows enough zonal wind variability in the tropical Pacific to trigger some ENSO warm events. The variability over the tropical Indian Ocean is also improved, mainly by a reduction of the equatorial westerly winds over the western part of the basin.

The better performance of Cy32r3 with respect to previous cycles is also found for near-surface temperatures at both the global scale and regional level (not shown). Global-mean temperature differences with the observations are consistently smaller than 1 K. However, the Northern Hemisphere continents show a warm bias while the ocean surfaces, especially over the tropics, remain too cold. It is likely that the continental biases are linked to deficiencies in the simulation of the snow cover and feedbacks related to soil moisture.

# 8 Conclusions

Revisions to the convection and diffusion parametrizations of the IFS have been presented that lead to higher and more realistic levels of atmospheric activity/variability in middle latitudes and the Tropics. The models mean state and variability have been evaluated on different time-scales by performing high-resolution deter-

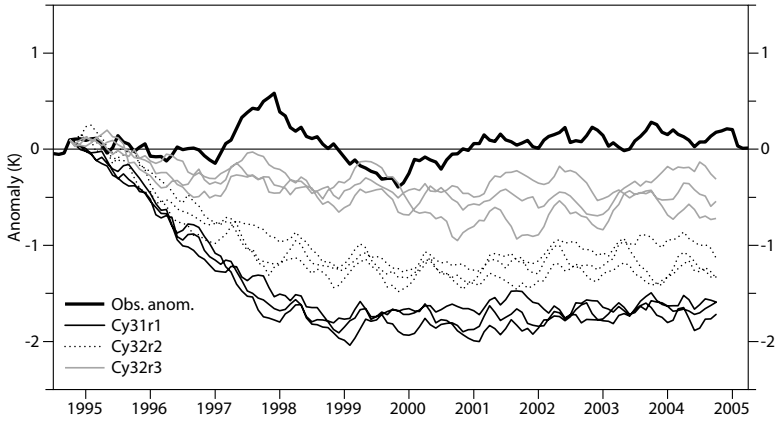


*Figure 16: Time series of the anomalies of sea surface temperature over the tropical Pacific (125°E-80°E,30°N-30°S) for ERA40 and three-ensemble simulations carried out with the IFS/HOPE coupled model. The anomalies have been computed as the difference between monthly-mean values and the mean seasonal cycle from ERA40 over the period 1970-2000. The three-member ensemble simulations start on the first of November 1994 and extend for 120 months.*

ministic and ensemble forecasts, monthly and seasonal integrations, as well as coupled decadal integrations, and by comparing them against available satellite and raingauge observations, operational analysis and 44-years of reanalysis statistics.

Model improvements concern in particular

- Midlatitude synoptic activity in the short and medium-range, as well as midlatitude cyclone statistics in seasonal forecasts.
- Increase in the amplitude of the annual cycle of tropical rainfall over land.
- Increased equatorial Kelvin wave activity, improved stratospheric climate, and (for the first time with the IFS) a realistic amplitude of the MJO during monthly integrations.
- Tropical SSTs in decadal integrations through more realistic wind forcing and radiative forcing (cloudiness).

Whereas the convection revisions in terms of entrainment and closure are mainly responsible for the changes in the rainfall pattern and the increase in tropical wave activity, the reduction in the vertical diffusion overall improved the representation of stratocumulus cloud decks, and contributed to an increase in middle latitude activity through an increase in the shear near the surface and at Jet Stream level. Overall the results confirm that a good representation of variability comes with a good representation of the mean state, and that improvements in the climate and the variability of the model through revisions to physical parametrizations (fast processes) should also be reflected in a reduction in short-range model errors (Rodwell and Palmer, 2007). If anything, the level of model activity in this latest cycle is slightly overestimated which somewhat penalises the deterministic RMS errors in the medium-range (Lorenc and Payne, 2007). The overestimation of activity seems to be related to an overestimation of mid-tropospheric moisture (in contrast to a too dry mid-troposphere in previous cycles), and possibly to an increase in wind shear near the top of the boundary-layer, and may enter the midlatitudes through the tropical forcing of extratropical Rossby waves.

Furthermore, the results suggest that it is possible to reasonably represent the atmospheric variability on a wide variety of time and space scales using a conventional set of physical parametrizations, without necessarily having to specifically use an explicit global representation of convection (e.g. Khairoutdinov et al., 2005).

This might come as a surprise, but considering that the modes discussed here are also eigenmodes of the (dry) atmosphere (Wedi and Smolarkiewicz, 2007), it seems reasonable to assume that it should be possible to develop a set of physical parametrizations that in some optimal way supports these modes. We do not yet fully understand why the current IFS cycle produces realistic Kelvin wave activity and previous cycles did not. But one requirement seems to be that the upper-tropospheric convective heating must be negatively correlated with the $\omega$ field of the wave, i.e. $-\overline{T'\omega'} > 0$ in order to convert available potential energy into kinetic energy (Steinheimer et al., 2008) and further sustain the wave; this is also supported by Shutts (2008) and current research by Slingo (personal communication).

Finally, the IFS is still unable to properly represent the stratospheric wind variability associated with the QBO, but in line with recent analysis and modelling studies (Horinouchi et al., 2003; Tindall et al., 2006) current developments indicate that this can be achieved with a scheme that parametrizes the drag induced by the higher frequency non-orographic gravity waves.

*Acknowledgements*

We are grateful to Anton Beljaars, Martin Miller and Philippe Bougeault for their guidance and encouragements in this work. We also greatly acknowledge the help of Rob Hine in figure drawing and the editing skills of Bob Riddaway.

# References

Adler SG, Huffman GJ, Chang A, Ferraro R, Xie P, Janowiak J, Rudolf B, Schneider U, Curtis S, Bolvin D, Gruber A, Susskind J, Arkin P. 2003. The Version 2 Global Precipitation Climatology Project (GPCP) Monthly Precipitation Analysis (1979–Present). *J. Hydrometeor.*, **4**, 1147–1167.

Anderson DLT, Stockdale T, Balmaseda MA, Ferranti L, Vitart F, Molteni F, Doblas-Reyes FJ, Mogensen K, Vidard A. 2007. Development of the ECMWF seasonal forecast System 3. *ECMWF Technical Memorandum 503* [Available from http://www.ecmwf.int/publications/library/do/references/show?id=87744].

Badger J., Hoskins BJ. 2000. Simple initial value problems and mechanisms for baroclinic growth. *J. Atmos. Sci.* **58:** 38–49.

Balmaseda MA, Vidard A, D.L.T. Anderson DLT. 2008. The ECMWF ocean analysis system ORA-S3. *Mon. Wea. Rev.* (in press).

Beare RJ, Thorpe AJ, White AA. 2003. The predictability of extratropical cyclones: Nonlinear sensitivity to localized potential-vorticity perturbations. *Quart. J. Roy. Meteor. Soc.* **129:** 219–237.

Bechtold P, Chaboureau JP, Beljaars ACM, Betts AK, Köhler M, Miller M, Redelsperger JL. 2004. The simulation of the diurnal cycle of convective precipitation over land in global models. *Quart. J. Roy. Meteor. Soc.* **130:** 3119–3137.

Berner J, Doblas-Reyes FJ, Palmer TN, Shutts G, Weisheimer W. 2008. Impact of a cellular automaton backscatter scheme on the systematic error and seasonal prediction skill of a global climate model. *Philosophical Transactions of the Royal Society B*, submitted.

Beljaars ACM, Viterbo P. 1999. The role of the boundary-layer in a numerical weather prediction model. Clear and cloudy boundary-layers. A. A. M. Holtslag and P. G. Duynkerke (eds.), *North Holland publishers*.

Betts AK, Ball JH, Viterbo P, Dai A, Marengo JA. 2005. Hydrometeorology of the Amazon in ERA-40. *J. Hydrometeoro* **6:** 764–774. Also ERA-40 Project Report 22.

Boville BA. 1984. The Influence of the Polar Night Jet on the tropospheric circulation in a GCM. *J. Atmos. Sci.* **41:** 1132–1142.

Buizza R, Houtekamer PL, Pellerin G, Toth Z, Zhu Y, Wei M. 2005. A comparison of the ECMWF, MSC, and NCEP global ensemble prediction systems *Mon. Wea. Rev.* **133:** 1076–1097.

Derbyshire SH, Beau I, Bechtold P, Grandpeix J-Y, Piriou J-M, Redelsperger J-L, PSoares PMM. 2004. Sensitivity of moist convection to environmental humidity. *Quart. J. Roy. Meteor. Soc.* **130:** 3055–3079.

Done JM, Craig GC, Gray SL, Clark PA, Gray MEB. 2006. Mesoscale simulations of organized convection: importance of convective equilibrium. *Quart. J. Roy. Meteor. Soc.* **132:** 737–756.

Edmon HJ, Hoskins BJ, McIntyre MW. 1981. Eliassen-Palm cross section for the troposphere. *J. Atmos. Sci.* **37:** 2600–2616.

Gill, A E. 1980. Some simple solutions for heat-induced tropical circulations. *Quart. J. Roy. Meteor. Soc.* **106:** 447–462.

Grabowski WW, Moncrieff MW. 2004. Moisture-convection feedback in the tropics *Quart. J. Roy. Meteor. Soc.* **130:** 3081–3104.

Håkånsson M. 2002. A two-dimensional numerical study of effects of vertical diffusion in frontal zones. *Quart. J. Roy. Meteor. Soc.* **128:** 2439–2467.

Haimberger L, Hantel M. 2000. Implementing convection into Lorenz's global cycle: Part. A new estimate of the conversion rate into kinetic energy. *Tellus* **52A:** 75–92.

Horinouchi T, and Coauthors. 2003: Tropical cumulus convection and upward-propagating waves in middle-atmospheric GCMs. *J. Atmos. Sci.* **60:** 2765–2782.

Jung, T. 2005: Systematic errors of the atmospheric circulation in the ECMWF forecasting system. *Quart. J. Roy. Meteor. Soc.* **131:** 1045–1073, 10.1256/qj.04.93.

Jung T, Barkmeijer J. 2006. Sensitivity of the tropospheric circulation to changes in the strength of the stratospheric polar vortex.*Mon. Wea. Rev.* **134:** 2191–2207.

Jung, T, Gulev SK, Rudeva I, Soloviov V. 2006: Sensitivity of extratropical cyclones characteristics to horizontal resolution in the ECMWF model. *Quart. J. Roy. Meteor. Soc.* **132:** 1839–1857, doi:1256/qj.05.212.

Khairoutdinov MF, Randall DA, DeMott C. 2005. Simulations of the atmospheric general circulation using a cloud-resolving model as a super-parameterization of physical processes *J. Atmos. Sci.* **62:** 2136–2154.

Leutbecher M, Palmer T. 2008. Ensemble forecasting. *J. Comput. Phys.* (in press) DOI: 10.106/j.jcp.2007.02.014.

Lorenc AC, Payne T. 2007. 4D-Var and the butterfly effect: Statistical four-dimensional data asimilation for a wide range of scales. *Quart. J. Roy. Meteor. Soc.* **133:** 607–614.

Lin J-L, Lee M-I, Kim D, Kang I-S, Frierson DMW. 2008. The impacts of convective parameterization and moisture triggering on AGCM-simulated convectively coupled equatorial waves. *J. Climate* (to appear).

Louis JF, Tiedtke M, Geleyn JF. 1982. A short history of the operational PBL parameterization at ECMWF. *Workshop on boundary layer parameterization*. ECMWF, 59–79.

Lopez P., Moreau E. 2005. A convection scheme for data assimilation. *Quart. J. Roy. Meteor. Soc.* **131:** 409–436.

Masunaga H. 2007. Seasonality and regionality of the Madden-Julian oscillation, Kelvin wave and equatorial Rossby wave. *J. Atmos. Sci.* **64:** 4400–4416.

Morcrette J-J, Barker HW, Cole JNS, Iacono MH, Pincus R. 2008. Impact of a new radiation package, McRad, in the ECMWF Integrated Forecasting System. *Mon. Wea. Rev.*

Peixoto JP, Oort AH. 1992. Physics of climate. *American Institute of Physics*. 520 pp.

Riciardulli L, Garcia RR. 2000. The excitation of equatorial waves by deep convection in the NCAR community climate model (CCM3).

Rodwell MJ, Palmer TN. 2007. Using numerical weather prediction to assess climate models. *Quart. J. Roy. Meteor. Soc.* **133:** 129–146.

Scinoccia JF, McFarlane NA. 2004. The variability of modeled tropical precipitation. *J. Atmos. Sci.* **61:** 1993–2015.

Shutts G. 2008. The forcing of large-scale waves in an explicit simulation of deep tropical convection. *Dyn. Atmos. Oceanc* (in press)

Simmons AJ, Hollingsworth A. 2002. Some aspects of the improvement of skill of numerical weather prediction.*Quart. J. Roy. Meteor. Soc.* **128:** 647–677.

Skamarock WC. 2004. Evaluating mesoscale NWP models using kinetic energy spectra. *Mon. Wea. Rev.* **132:** 3019–3032

Slingo J, Blackburn M, Betts A, Brugge R, Hodges K, Hoskins B, Miller M, Steenman-Clark L, Thuburn J. 1994. Mean climate and transience in the tropics of the UGAMP GCM: Sensitivity to convective parametrization. *Quart. J. Roy. Meteor. Soc.* **120:** 881–922.

Sobel AH, Nilsson J, Polvani LM. 2001. The week temperature gradient approximation and balanced tropical moisture waves. *J. Atmos. Sci.* **58:** 3650–3665.

Steinheimer M, Hantel M, Bechtold P. 2008. Convection in Lorenz's global energy cycle with the ECMWF model. *Tellus* (in press), also available as *ECMWF Technical Memorandum 545* from http://www.ecmwf.int/publications/library/do/references/list/14

Simmons AJ, Hollingsworth A. 2002. Some aspects of the improvement of skill of numerical weather prediction. *Quart. J. Roy. Meteor. Soc.* **132:** 1917–1932.

Tindall JC, Thuburn J, Highwood EJ. 2006. Equatorial waves in the lower startosphere. II: Annual and interannual variability. *Quart. J. Roy. Meteor. Soc.* **131:** 195–212.

Uppala S, Kallberg PW, Simmons AJ, Andrae U, Da Costa Bechtold V, Fiorino M, Gibson JK, Haseler J, Hernandez A, Kelly GA, Li X, Onogi K, Saarinen S, Sokka N, Allan RP, Andersson E, Arpe K, Balmaseda MA, Beljaars ACM, van de Berg L, Bidlot J, Bormann N, Caires S, Chevallier F, Dethof A, Dragosavac M, Fisher M, Fuentes M, Hagemann S, Holm E, Hoskins BJ, Isaksen L, Janssen PAEM, Jenne R, McNally AP, Mahfouf J-F, Morcrette J-J, Rayner NA, Saunders RW, Simon P, Sterl A, Trenberth KE, Untch A, Vasiljevic D, Viterbo P, and Woollen J. 2005. The ERA-40 re-analysis *Quart. J. Roy. Meteor. Soc.* **131:** 2761–2779.

Wedi NP, Smolarkiewicz PK. 2007. A reduced model of the Madden-Julian oscillation. *Int. J. Numer. Meth. Fluids*, published online DOI:10.1002/fld.1612.

Wheeler MC, Hendon HH. 2004. An all-season real-time multivariate MJO index: Development of an index for monitoring and prediction. *Mon. Wea. Rev.* **132:** 1917–1932.

Wheeler MC, Weickmann K. 2001. Real-time monitoring and prediction of modes of coherent synoptic to intraseasonal tropical variability. *Mon. Wea. Rev.* **129:** 2677-2694.

Wheeler MC, Kiladis GN. 1999. Convectively coupled equatorial waves: Analysis of clouds and temperature in the wavenumber-frequency domain. *J. Atmos. Sci.* **56:** 374–399.

Wilks SD.1995. Statistical methods in the atmospheric sciences. *Academic Press*. 467 pp.

Ẑagar NE, Andersson E, Fisher M. 2005. Balanced tropical data assimilation based on a study of equatorial waves in ECMWF short-range forecast errors. *Quart. J. Roy. Meteor. Soc.* **131:** 987–1011.